AtALMT5 mediates vacuolar fumarate import and regulates the malate/fumarate balance in Arabidopsis

Roxane Doireau, Justyna Jaślan, Paloma Cubero-Font, Elsa Demes-Causse, Karen Bertaux, Cédric Cassan, Pierre Pétriacq, Alexis de Angeli

New Phytologist

Research

*At*ALMT5 mediates vacuolar fumarate import and regulates the malate/fumarate balance in Arabidopsis

Roxane Doireau[1]*, Justyna Jaślan[1]*, Paloma Cubero-Font[1]*, Elsa Demes-Causse[1], Karen Bertaux[1], Cédric Cassan[2,3], Pierre Pétriacq[2,3] and Alexis De Angeli[1]

[1]IPSiM, Univ Montpellier, CNRS, INRAE, Institut Agro, 34060, Montpellier, France; [2]UMR BFP, University Bordeaux, INRAE, 33882, Villenave d'Ornon, France; [3]Bordeaux Metabolome, MetaboHUB, PHENOME-EMPHASIS, 33140, Villenave d'Ornon, France

Author for correspondence:
Alexis De Angeli
Email: alexis.deangeli@cnrs.fr

Received: *3 July 2024*
Accepted: *9 August 2024*

New Phytologist (2024)
doi: 10.1111/nph.20077

Key words: *Arabidopsis thaliana*, carbon sink, ion transporter, organic acids, stomata, vacuole.

Summary

- Malate and fumarate constitute a significant fraction of the carbon fixed by photosynthesis, and they are at the crossroad of central metabolic pathways. In *Arabidopsis thaliana*, they are transiently stored in the vacuole to keep cytosolic homeostasis.
- The malate and fumarate transport systems of the vacuolar membrane are key players in the control of cell metabolism. Notably, the molecular identity of these transport systems remains mostly unresolved. We used a combination of imaging, electrophysiology and molecular physiology to identify an important molecular actor of dicarboxylic acid transport across the tonoplast.
- Here, we report the function of the *A. thaliana* Aluminium-Activated Malate Transporter 5 (*At*ALMT5). We characterised its ionic transport properties, expression pattern, localisation and function *in vivo*. We show that *At*ALMT5 is expressed in photosynthetically active tissues and localised in the tonoplast. Patch-clamp and *in planta* analyses demonstrated that *At*ALMT5 is an ion channel-mediating fumarate loading of the vacuole. We found in *almt5* plants a reduced accumulation of fumarate in the leaves, in parallel with increased malate concentrations.
- These results identified *At*ALMT5 as an ion channel-mediating fumarate transport in the vacuoles of mesophyll cells and regulating the malate/fumarate balance in Arabidopsis.

Introduction

In plants, malate, fumarate and citrate have central functions in cell metabolism. These organic acids are involved in metabolic pathways such as the synthesis and degradation of starch and sugars, in cellular respiration and in photosynthetic carbon fixation. A significant part of the carbon fixed during photosynthesis in plant cells is stored as malate and, in some plant species including *Arabidopsis thaliana*, also as fumarate (Chia *et al.*, 2000). Additionally, citrate, malate and fumarate are involved in amino acid biosynthesis, the regulation of cellular pH (Hurth *et al.*, 2005) and tolerance to heavy metal (Sasaki *et al.*, 2004). In guard cells, malate is part of the molecular mechanisms regulating the opening and the closure of stomata (Roelfsema & Hedrich, 2005; Fernie & Martinoia, 2009; Araújo *et al.*, 2011; Meyer *et al.*, 2011).

In some plants, including *A. thaliana*, fumarate and malate are accumulated at similar levels, and together they form the major pool of C_4-organic acids in plant cells (Zell *et al.*, 2010). Malate and fumarate are metabolically connected through fumarase enzymes, which reversibly converts malate into fumarate. Remarkably, in *A. thaliana*, two fumarase isoforms exist, the Fumarase 1 (FUM1, *At*2g47510) and the Fumarase 2 (FUM2, *At*5g50950). FUM1 is localised in the mitochondria and is part of the Krebs cycle (Heazlewood & Millar, 2005) while FUM2 is a cytosolic enzyme (Pracharoenwattana *et al.*, 2010). The function of the FUM2 is associated with the accumulation of fumarate in mesophyll cells (Pracharoenwattana *et al.*, 2010). Such an accumulation seems to be linked to the adaptation to low temperature and water restriction (Muller *et al.*, 2011; Saunders *et al.*, 2022). Recent reports using metabolic flux modelling propose that the conversion of malate into fumarate is a metabolic fail-safe to keep malate at levels in the cytosol (Saunders *et al.*, 2022). Indeed, because of its central role in plant metabolism, cytosolic malate needs to be tightly regulated. Therefore, the reversible conversion of cytosolic malate into fumarate by FUM2 keeps cytosolic malate at metabolically compatible levels. Since malate and fumarate are mainly stored in the vacuole, their transport across the tonoplast regulates cytosolic homeostasis (Hurth *et al.*, 2005; Medeiros *et al.*, 2017). Being the principal store of malate and fumarate, the vacuole is part of the mechanisms regulating plant cell metabolism (Martinoia *et al.*, 2007). The vacuolar concentration of these organic acids follows the circadian cycle, with malate and fumarate stored in the vacuole

*These authors contributed equally to this work.

during daytime and remobilised at night for cellular respiration (Gibon *et al.*, 2009). Instead, citrate, a major product of the Krebs cycle, is stored in the vacuole during the night and remobilised during the day and is a source of carbon skeletons for light-dependent nitrate assimilation (Tcherkez *et al.*, 2012; Cheung *et al.*, 2014; Winter & Smith, 2022).

Different transport systems mediate the fluxes of metabolites across the tonoplast. The first vacuolar organic acid transporter identified, *At*DT, was associated with the control of pH homeostasis and in storing/remobilising dicarboxylates in the vacuole (Hurth *et al.*, 2005). *At*DT catalyses the exchange of vacuolar malate with cytosolic citrate (Frei *et al.*, 2018). In the leaves, *Attdt* knock-out plants present reduced malate and fumarate content compared with wild-type (WT), but increased citrate (Medeiros *et al.*, 2017; Frei *et al.*, 2018).

The ion channels of the Aluminium-Activated Malate Transporter (ALMT) family are able to mediate malate and fumarate transport. The ALMTs are membrane proteins present only in plants and, in Arabidopsis, the 14 members are divided in three clades (Kovermann *et al.*, 2007). The members of the ALMT family are involved in a variety of functions, including tolerance to aluminium in the soil, mineral nutrition, regulation of fruit acidity (Sharma *et al.*, 2016; Li *et al.*, 2020), ion homeostasis and stomatal aperture regulation (Meyer *et al.*, 2011; De Angeli *et al.*, 2013; Eisenach *et al.*, 2017; Sasaki *et al.*, 2022). Clade I is formed by six ALMTs localised at the plasma membrane, and it includes the first identified *At*ALMT, *At*ALMT1 (Sasaki *et al.*, 2004). In the roots, *At*ALMT1 mediates malate efflux to chelate aluminium in the soil, conferring Al^{3+} tolerance. Clade III is formed by four members and includes the plasma membrane ion channel *At*ALMT12 that is involved in the regulation of stomatal aperture (Meyer *et al.*, 2010; Sasaki *et al.*, 2022). Finally, Clade II presents three members: *At*ALMT4, *At*ALMT6 and *At*ALMT9, localised at the vacuolar membrane and one, *At*ALMT3, localised at the plasma membrane (Meyer *et al.*, 2011; De Angeli *et al.*, 2013; Baetz *et al.*, 2016; Eisenach *et al.*, 2017; Maruyama *et al.*, 2019). *At*ALMT9 is expressed in the roots and the shoots (Baetz *et al.*, 2016). In the leaves, it can mediate malate influx in the vacuole of mesophyll cells, and in guard cells, it most likely mediates chloride uptake in the vacuole during stomatal opening (De Angeli *et al.*, 2013). *At*ALMT4 mediates the efflux of malate from the vacuole and regulates abscisic acid (ABA)-induced stomatal closure (Eisenach *et al.*, 2017). Finally, *At*ALMT6 is specifically expressed in guard cells and mediates both malate influx and efflux from the vacuole and is activated by cytosolic Ca^{2+} (Meyer *et al.*, 2011; Ye *et al.*, 2021). However, even if electrophysiological approaches demonstrated that these vacuolar ALMTs are able to mediate malate and fumarate transport across the tonoplast, no significant difference in the content of these organic acids could be detected in the respective Arabidopsis knock-out mutants (Baetz *et al.*, 2016; Eisenach *et al.*, 2017). This keep the issue of their role *in vivo* as tonoplastic malate transport systems an open question.

Notably, *At*ALMT5 has been the forgotten member of Clade II, and almost no information about it is available. Indeed, its functional characteristics as well as its role *in vivo* are still unknown. Therefore, in this study, we decided to tackle the issue of the function of *At*ALMT5 in Arabidopsis. Our findings show that *At*ALMT5 is localised in the vacuolar membrane and is specifically expressed in the shoots. We found that *At*ALMT5 preferentially mediates fumarate currents in a physiological range of transmembrane potentials and that vacuoles from *almt5* mutants have reduced fumarate currents. We demonstrated that *in vivo* *At*ALMT5 mediates fumarate accumulation in the leaves and that in *almt5* knock-out plants, the malate/fumarate ratio is modified. Overall, our data identify *At*ALMT5 as a transporter-mediating fumarate transport across the vacuolar membrane of Arabidopsis. In the leaves, *At*ALMT5 regulates the accumulation of organic acids produced by photosynthesis.

Materials and Methods

Plant material and growth conditions

Arabidopsis thaliana (L.) Heynh. genotypes were as follows: Columbia-0 (Col-0), *almt5-1* (WiscDSLox386E04.0), *almt5-2* (GK-696G03), *almt9-1* (SALK_055490), OST2-2D (EMS mutant; Merlot *et al.*, 2007), *fum2-1* (SALK_025631.23.65.x) and *fum2-2* (GK-107E05). *Arabidopsis thaliana* plants were grown in pots in a growth chamber with day : night regime of 8 h : 16 h, 25°C : 20°C, 65% humidity and LED lights 150 µmol m^{-2} s^{-1}. For seed propagation, plants were grown in a glasshouse. *In vitro A. thaliana* cultures were grown in ½-strength Murashige & Skoog (½MS) medium supplemented with 0.05% MES buffer, 1% sucrose and 0.7% (w/v) agar. Seeds were surface-sterilised, and grown in a growth chamber (day : night regime, 16 h : 8 h, 21°C : 21°C, 150 µmol m^{-2} s^{-1}). In all cases, seeds were stratified 72 h at 4°C in the dark. *Nicotiana benthamiana* Domin plants were grown on soil (day : night regime of 16 h : 8 h, 22°C : 20°C, 65% humidity and photon flux density of 150 µmol m^{-2} s^{-1}).

Molecular biology, plant transformation and selection

The genomic fragments *gALMT5* and *gALMT9* were amplified from Col-0 using primers with *AttB1* and *AttB2* flanking sequences for cloning with Gateway technology (Invitrogen). The *gALMT5* and *gALMT9* fragments were cloned with and without the stop codon by polymerase chain reaction (PCR) with specific primers (Supporting Information Table S2). The PCR products were cloned into the pDONR201 or pDONR223 vectors and then in the corresponding destination vector by Gateway technology (Invitrogen, Thermo Fisher Scientific Inc., Waltham, MA USA). The *gALMT5* and *gALMT9* fragments gene with the STOP codon were cloned into the pCOP destination vector, and the genomic *AtALMT5* gene without the STOP codon into pMOP destination vector. pMOP and pCOP are binary vectors derived from the pMDC83 (Curtis & Grossniklaus, 2003). In pCOP, the 35S promoter and the GFP (Green Fluorescent Protein) were removed, and in pMOP, only the 35S promoter was removed.

For β-glucuronidase (GUS) reporter gene expression analyses, a 1846-bp fragment preceding the start codon of *AtALMT5* was amplified by PCR using specific primers with *AttB1* and *AttB2* flanking sequences (Table S2) and cloned into the pMDC163

(Curtis & Grossniklaus, 2003) destination vector, resulting in a transcriptional fusion of *AtALMT5* promoter with GUS.

For transient overexpression of the *At*ALMT5 in mesophyll cells from *N. benthamiana* leaves, the *ALMT5* cDNA was amplified by PCR with specific primers (Table S2). The PCR product was finally cloned in pMDC43 and pMDC83 destination vectors (Curtis & Grossniklaus, 2003) for GFP C- and N-terminal fusion, respectively.

For transformation of WT (Col-0) plants with *pALMT5:GUS* and for the complementation of *almt5-1* with *gALMT5* and *gALMT5-GFP* and *almt9-1* with *gALMT9* and *gALMT9-GFP* constructs, plants were transformed with *Agrobacterium tumefaciens* using floral dip method (Clough & Bent, 1998). Transgenic lines were selected until the T3 generation in ½MS agar plates using hygromycin antibiotic.

Screening of T-DNA insertion lines by PCR

T-DNA insertion lines were screened by PCR to confirm the presence of the T-DNA and to verify that they were homozygous T-DNA insertion lines for *AtALMT5*. For this purpose, DNA extraction from leaves was performed with the REDExtract N-Amp™ Plant PCR kit (Sigma-Aldrich Co.) followed by the PCR with the GoTaq® DNA Polymerase (Promega) and specific primers (Table S2).

Histochemical localisation of *At*ALMT5 promoter activity

For GUS histochemical activity (Jefferson, 1987), samples were fixed in 90% (v/v) acetone for 20 min. GUS activity in plant tissues was visualised after vacuum-infiltration of the staining buffer (50 mM $NaPO_4$ pH 7, 2 mM $K_3Fe[CN]_6$, 2 mM $K_4Fe[CN]_6$, 0.2% Triton X-100) containing 1 mM 5-bromo-4-chloro-3-indolyl-β-D-glucuronide as a GUS substrate for 2 min and 4 h staining at 37°C. Chlorophyll was removed with 70% (v/v) ethanol. Two independent *AtALMT5* promoter-GUS transgenic lines were analysed at T3 generation. Images were acquired with an Axiozoom v.16 (Zeiss) macroscope using the ZEN Software (Zeiss).

Fluorescence microscopy

GFP fluorescence in *almt5-1/gALMT5-GFP* and *almt9-1/gALMT9-GFP* T3 transgenic plant lines was observed under ZEISS Axio Observer (Carl Zeiss). Three independent T3 plant lines were observed. Roots and leaves samples were observed with 470/40 nm excitation and 525/50 nm emission filter sets.

An inverted Leica SP8 (Leica, Mannheim, Germany) Confocal Laser Scanning Microscope was used for subcellular localisation in *A. thaliana* and *N. benthamiana*. Fluorescence was detected using a GaAsP Hybrid photon detector in photon counting mode. The GFP fluorescence detected in the 500–550 nm range after excitation at 488 nm with an Argon laser. Chlorophyll autofluorescence was detected in the 600–650 nm emission range after excitation at 488 nm. Images were acquired with a ×63 oil objective (HCX Plan Apochromat CS 1.4 NA; Leica) and processed using the IMAGEJ software package.

Electrophysiology

Currents were recorded using an EPC-10 amplifier (HEKA Electronics, Lambrecht/Pflaz, Germany). Data were acquired and analysed using PATCHMASTER and FITMASTER softwares (HEKA). Microelectrodes (resistance 2.5–5 MΩ) prepared from GC150TF-15 glass capillaries (Harvard Apparatus, Holliston, MA, USA), treated with sigmacote (Sigma-Aldrich Co.) and coated with Sylgard (WPI, Friedberg, Germany). The reference electrode was placed in 1 M KCl agar bridge with 2% agar. Vacuolar side buffer: 11.2 mM DL-malic acid, 100 mM HCl, pH 6 with BisTrisPropane (BTP), π = 550 mOsmol kg^{-1}. The cytosolic side buffers were composed of (1) 100 mM HCl, 0.1 mM $CaCl_2$ and supplemented with 1 mM malate or 1 mM fumarate as indicated; (2) 100 mM DL-malic acid, 0.1 mM $CaCl_2$; and (3) 100 mM fumaric acid and 0.1 mM $CaCl_2$. For all cytosolic side buffers, pH 7.5 was adjusted with BTP and π = 500 mOsmol kg^{-1} with D-sorbitol. The cytosolic side buffers were exchanged using a gravity-driven perfusion system. In recordings from *N. benthamiana*, the vacuoles expressing the gene of interest were selected based on fluorescence with an epifluorescence microscope (Axiobserver; Zeiss). Current recordings were conducted on excised patch cytosolic-side-out configuration. Currents were recorded with the following voltage-pulse protocol: after a 300 ms prepulse at +80 mV, we applied a 3000 ms pulses from +40 to −120 mV in −20 mV steps, followed by a tail pulse at +80 mV. Holding potential was 0 mV, and currents were recorded at a sampling rate of 100 µs and low-pass filtered at 2.9 kHz. All recordings started in the cytosolic condition (1). The liquid junction potential measured was ±2 mV and was not corrected. In recordings from *A. thaliana* vacuoles, ion current were recorded in the whole-vacuole configuration. Measurements were done 12 min after the establishment of the whole-vacuole configuration to ensure dialysis of the vacuolar lumen. Currents were recorded using a voltage-pulse protocol starting at a holding voltage of 0 mV, 2000-ms-lasting voltage pulses were applied in the range of +33 to −127 mV in −20 mV increments, a post-pulse was applied at +33 mV for 500 ms and back to the holding voltage of 0 mV. Currents were recorded at a sampling rate of 100 µs and low-pass filtered at 1 kHz. Currents were evoked in the cytosolic conditions (2) or (3). In these conditions, the liquid junction potential measured were +7 mV and was corrected. Patch-clamp data are presented according to the endomembrane convention for electrical measurements (Bertl *et al.*, 1992).

Stomatal aperture and rosette water loss assays

For stomatal opening measurements, leaves of 4- to 5-wk-old plants were taken 1 h before the end of the dark period and prepared under green light. The abaxial side of the leaf was glued on a coverslip using medical adhesive (Hollister Adapt™ 7730, Libertyville, IL, USA). The adaxial part and the mesophyll cells were gently removed, and the epidermis was covered with a stomatal opening solution (30 mM KCl, 5 mM MES, 0.1 mM $CaCl_2$, pH 5.7). The sample was incubated 20 min in the dark and illuminated for 3 h (LED-240 µmol m^{-2} s^{-1}). For each leaves, 40

stomata at each time point were imaged on a Zeiss Observer microscope with a ×40 objective (Plan Apochromat ×40/1.3 Oil DIC (UV) VIS IR). Stomatal aperture was measured using the ImageJ software. Leaves from knock-out and WT plants were analysed in parallel. For each leaf and genotype, the mean stomata aperture was calculated. Experiments were conducted blind until the end of the analysis.

For rosette dehydration experiments, the rosette of 5-wk-old Arabidopsis plants was detached at the level of the petiole. Glycerine was placed to avoid water loss at the cutting site. The rosette was placed upside down on a balance (Ohaus, Parsippany, NJ, USA) illuminated by a light placed on the top, and the weight was automatically recorded each 10 s for 40 min. The temperature was 25°C and RH was 64% and constantly monitored with a detector (Trotec BL30, Heinsberg, Germany).

Anion content measurement by high pressure ion chromatography (HPIC)

Leaves no. 9 from 12 plants of 40-d-old plants were collected 5 h after the beginning of light period in the growth chamber. The leaves were frozen at −20°C for 20 min, heated to 70°C for 30 min with 1 ml mQ water and centrifuged at 18 000 ***g*** at 4°C for 15 min. The supernatant collected was analysed in 1.5-ml vial kit for Dionex® (ThermoFisher Scientific). Analysis was done by HPIC (Dionex™ ICS-5000+ Capillary HPIC™) using the software Chromeleon 7 (ThermoFisher).

Metabolite extraction

For metabolome analysis, leaves 8 and 9 of Arabidopsis rosettes were used. Leaves were rapidly collected into 2-ml microtubes, then flash-frozen in liquid nitrogen. They were then dried by lyophilisation. Metabolite extraction was done following the protocol described previously (Luna *et al.*, 2020).

Targeted biochemical phenotyping

Targeted analyses of sucrose, fructose, glucose and starch were conducted on the HiTMe plateau at Bordeaux Metabolome Facility. Measurements were based on coupled enzyme assays as described previously (Gibon *et al.*, 2002; Biais *et al.*, 2014).

Statistical analysis

All statistical analyses were performed using the nonparametrical Mann–Whitney test, significance levels are noted as *, $P < 0.05$; **, $P < 0.01$; ***, $P < 0.001$.

Results

*At*ALMT5 is localised in the vacuolar membrane and expressed in mesophyll and in guard cells

To understand the role of *At*ALMT5 (AT1G68600), we started investigating its tissue-specific expression pattern. We generated a transcriptional fusion of the promoter region (i.e. 1715 bp upstream of the start codon; *pALMT5*) with the GUS reporter. The *At*ALMT5 promoter activity was detected through GUS staining. The analysis was performed at 2, 3, 6, 9, 12 and 15 d after sowing (DAS) transgenic lines expressing *pALMT5:GUS* (Fig. S1a–f). GUS staining was found in the vasculature of the cotyledons 2 DAS, and from 3 DAS in the mesophyll tissue (Fig. S1a,b). Later in the development, *pALMT5* was active in the mesophyll and in the stomata (Figs 1a *middle*, S1i,j). In the roots, we observed GUS staining in the vascular tissues of the primary (Fig. 1a *top*, *right*) and secondary roots (Fig. S1k). Notably, no GUS staining was detected in the root tip (Figs 1a *bottom*, *right*, S1l).

To analyse the subcellular localisation of *At*ALMT5, we generated N- and C-terminal GFP fusions with the cDNA of *At*ALMT5 under the control of the CaMV 35S promoter. We transiently expressed the *GFP-ALMT5* and *ALMT5-GFP* in *N. benthamiana* leaves (Fig. S2a,b) and extracted mesophyll protoplasts to isolate vacuoles. Confocal imaging shows tonoplastic GFP fluorescence with both *At*ALMT5 N- and C-terminal fusions (Fig. S2b *top* and *middle*). We observed a residual GFP fluorescence in endomembranes after protoplast burst that is likely due to the overexpression (Fig. S2b *bottom*). To exclude bias from overexpression in heterologous systems, we analysed the subcellular localisation of *At*ALMT5 in Arabidopsis. Therefore, we selected transgenic lines expressing the genomic fragment, including the promoter region, of *AtALMT5* fused to the GFP (*gALMT5-GFP*; see the Materials and Methods section). We compared vacuoles isolated from Arabidopsis mesophyll protoplasts obtained from WT untransformed plants with plants expressing *gALMT5-GFP* (Figs 1b, S2c). Notably, we found that *At*ALMT5-GFP is localised in the tonoplast as demonstrated by GFP fluorescent signal in the vacuolar membrane (Figs 1b, S2c). In mesophyll cells, after the isolation of the vacuole, we only observed a weak residual GFP signal in the other endomembranes after protoplasts burst (Fig. S2c).

To analyse the expression pattern of *At*ALMT5, we used the transgenic lines expressing *gALMT5-GFP*. In parallel, we analysed WT (i.e. negative control) and *gALMT9-GFP* expressing plants (i.e. positive control; see Methods S1). We observed the fluorescence 7 DAS in *gALMT5-GFP* and *gALMT9-GFP* transgenic lines (Figs 1c, S3). In plants expressing *gALMT9-GFP*, GFP fluorescence was observed in the tonoplast all over the root (Figs 1c, S3 *bottom*). Differently, in *gALMT5-GFP* roots, we observed fluorescence in the same range of the autofluorescence levels found in the roots of WT (Fig. 1c *top* and *middle*). This differed with the promoter activity revealed by GUS staining (Fig. 1a). This difference between the protein expression pattern revealed by *gALMT5-GFP* and the promoter activity pattern from *pALMT5:GUS* likely resulted from *cis*-regulatory elements present in the intronic regions of the *gALMT5* genomic fragment (Kaufmann *et al.*, 2010). Accordingly, transcriptomic (http://ipf.sustech.edu.cn/pub/athrdb/) and reverse transcription polymerase chain reaction (Maruyama *et al.*, 2019) data found *AtALMT5* transcripts only in the shoots. In the leaves, we found *AtALMT5* expression in the stomata, in the epidermal cells

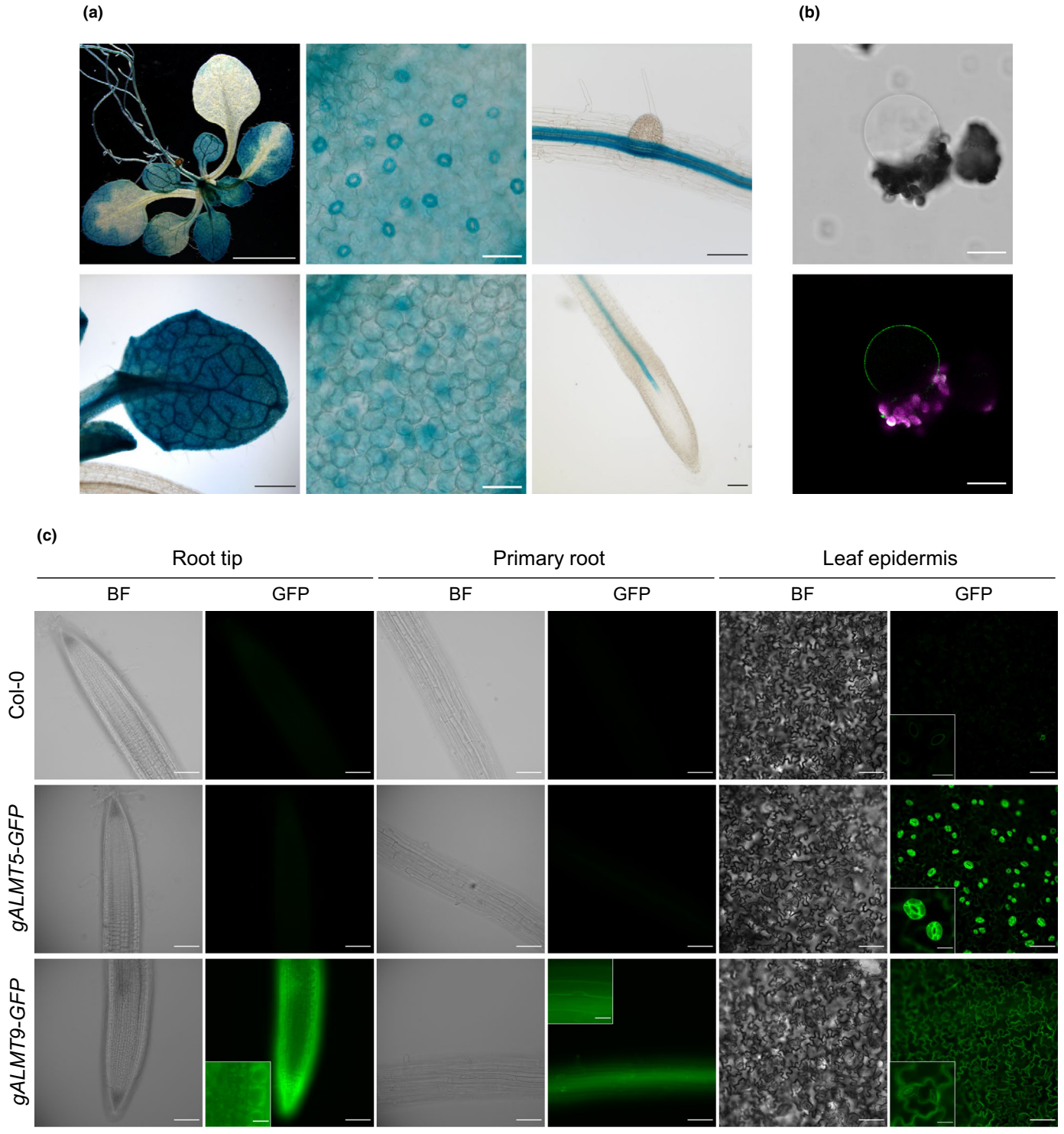

Fig. 1 Tissue and cellular expression of Aluminium-Activated Malate Transporter 5. (a) Representative β-glucuronidase (GUS) staining in *Arabidopsis thaliana* Col-0 plants transformed with *pALMT5:GUS*. Rosette from a 15-d-old plant (*top*, *left panel*; Bar, 4 mm). Leaf from a 12-d-old rosette (*bottom*, *left panel*; Bar, 500 μm) shows GUS staining in stomata (*top*, *middle panel*) and in mesophyll cells (*bottom*, *middle panel*; Bar, 50 μm). In the root, GUS staining is observed in the central cylinder (*top*, *right panel*; Bar, 100 μm) but not at the root tip (*bottom*, *right panel*; Bar, 100 μm). (b) Confocal images of a vacuole released from Arabidopsis mesophyll protoplast isolated from *almt5-1::ALMT5-GFP* transgenic plants. Transmitted light image (*top*); GFP fluorescence was detected after excitation at 488 nm and emission at 500–550 nm (*bottom*). Green represents GFP florescence and magenta the chloroplasts. Bars, 20 μm. (c) *gALMT5-GFP L11-20*, and *gALMT9-GFP L2-16* expression in 7-d-old transgenic Arabidopsis seedlings. Comparison between the fluorescence (Ex 470/40 nm, Em 525/50 nm) observed in wild-type (*top*), *gALMT5-GFP L11-20* (*middle*) and *gALMT9-GFP L2-16* (*bottom*). *gALMT5-GFP* fluorescence was detected in the epidermis and in stomata (*inset*). Differently, *gALMT9-GFP* fluorescence was detected in the roots and in the epidermis. Bars: 100 μm; (insets) 20 μm.

(Figs 1c, S3) and mesophyll cells (Fig. 1b). *AtALMT9* expression was observed in epidermal cells (Figs 1c, S3).

Our data show that, while *At*ALMT9 is expressed all over the plant, *At*ALMT5 is almost exclusively expressed in the aerial parts of Arabidopsis. Therefore, *At*ALMT5 is, like its homologues *At*ALMT4, *At*ALMT6 and *At*ALMT9 (Kovermann *et al.*, 2007; Meyer *et al.*, 2011; Eisenach *et al.*, 2017), localised in the tonoplast at the level of the shoots in Arabidopsis.

*At*ALMT5 mediates malate and fumarate currents directed to the vacuole

To characterise the transport properties of *At*ALMT5, we applied the patch-clamp technique to *N. benthamiana* vacuoles overexpressing *At*ALMT5-GFP and compared with *At*ALMT9-GFP (De Angeli *et al.*, 2013; Zhang *et al.*, 2013). We conducted patch-clamp experiments in cytosolic-side-out configuration and recorded macroscopic currents (Figs 2, S4; De Angeli *et al.*, 2013; Baetz *et al.*, 2016; Eisenach *et al.*, 2017). In order to highlight anion currents and minimise cation ones, we designed measuring buffers using as major cation BTP that does not permeate across the vacuolar membrane (De Angeli *et al.*, 2013; Carpaneto *et al.*, 2017; Eisenach *et al.*, 2017). So far, the characterised vacuolar *At*ALMTs are permeable to malate, fumarate and chloride (Kovermann *et al.*, 2007; Meyer *et al.*, 2011; De Angeli *et al.*, 2013; Eisenach *et al.*, 2017). We first tested the capacity of *At*ALMT5 to mediate the transport of malate and fumarate, the two main C_4 organic acids stored in the vacuoles of *A. thaliana* (Hurth *et al.*, 2005). We therefore recorded ionic currents in vacuolar patches overexpressing *At*ALMT5 and *At*ALMT9 in the presence of 100 mM $malate_{cyt}$ and of 100 mM $fumarate_{cyt}$ in the cytosolic side buffer. In both conditions, the vacuolar side buffer was the same (see the Materials and Methods section). In vacuolar patches overexpressing *At*ALMT5 in presence of 100 mM $malate_{cyt}$, we observed inward currents (i.e. malate currents directed to the vacuole) with a mean amplitude of −256 ± 66 pA at −120 mV (Fig. 2a,c). In the same conditions, patches overexpressing *At*ALMT9 presented a mean current amplitude of −955 ± 105 pA at −120 mV, a value significantly higher than for *At*ALMT5 ($P = 0.005$ with a *t*-test; Fig. 2a,d). Both *At*ALMT5- and *At*ALMT9-mediated malate currents were inward rectifying and displayed time-dependent kinetics. Since malate or fumarate were the only anions present in the cytosolic buffers, they mediated the measured inward currents. Additionally, *At*ALMT5 currents presented a time-independent current component visible just after the application of the voltage step (Fig. 2a,b). Further, compared with *At*ALMT9, *At*ALMT5 malate currents were activated at more negative membrane potentials (i.e. below −40 mV; Fig. 2c,d). In the presence of 100 mM $fumarate_{cyt}$, vacuolar patches overexpressing *At*ALMT5 had a mean inward rectifying current amplitude of −690 ± 68 pA at −120 mV (Fig. 2c), which is 2.7 times more than in 100 mM $malate_{cyt}$ (Fig. 2c). Importantly, *At*ALMT5-mediated fumarate currents could be detected in the physiological range of the vacuolar membrane potentials, between 0 and −50 mV (Konrad & Hedrich, 2008). In comparison, in the

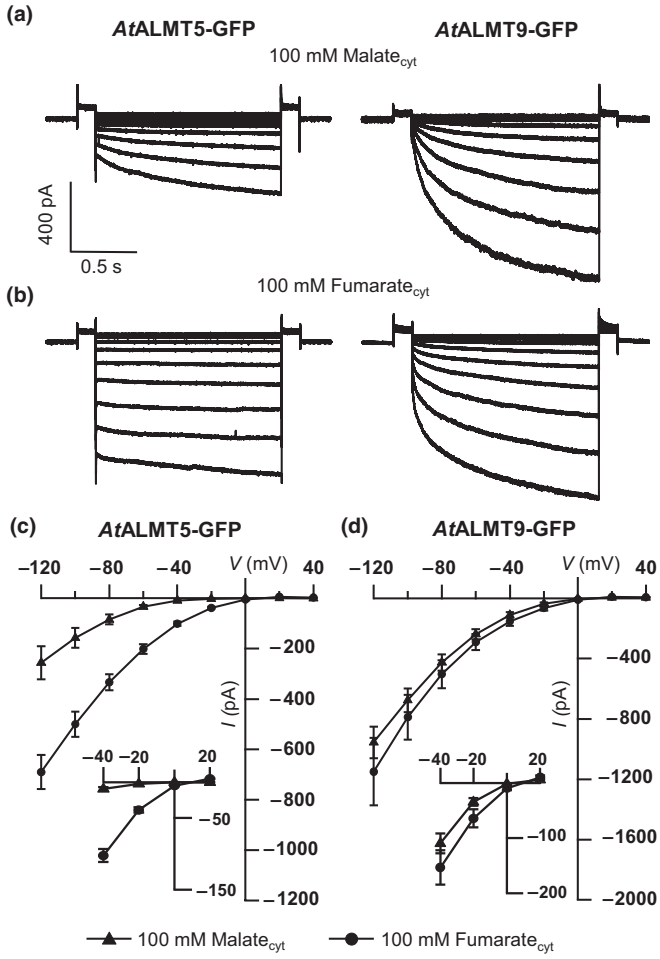

Fig. 2 Patch-clamp analysis of *At*ALMT5 ion transport proprieties. (a, b) Representative currents in cytosolic-side-out patches from *Nicotiana benthamiana* mesophyll vacuoles overexpressing *At*ALMT5-GFP or *At*ALMT9-GFP under different cytosolic conditions as indicated. (c, d) *At*ALMT9-GFP and *At*ALMT5-GFP steady-state currents plotted against membrane voltages in presence of 100 mM malatecyt in the cytosolic solution (closed triangles; *At*ALMT9-GFP $n = 6$, *At*ALMT5-GFP $n = 5$) and in presence of 100 mM fumaratecyt in the cytosolic solution (closed circles; *At*ALMT9-GFP $n = 4$, for *At*ALMT5-GFP $n = 9$). Insets in (c, d) represent magnification of the currents in the −40 to +20 mV range. After a prepulse at +80 mV currents were recorded in response to voltage pulses from +40 mV until −120 mV in −20 mV steps followed by a step at +80 mV. The holding voltage was 0 mV. Data points represent means ± SEM.

presence of 100 mM $fumarate_{cyt}$, vacuolar patches expressing *At*ALMT9 had mean current amplitudes overlapping with malate currents at all tested membrane potentials (Fig. 2b,d). Notably, in contrast to *At*ALMT9, *At*ALMT5 fumarate currents did not display significant time-dependent component at any applied voltage (Fig. 2b). Control experiments in *N. benthamiana* mesophyll vacuoles from plants transformed with the p19 vector only (see Methods S1) displayed a negligible level of background currents (−8 ± 2 pA; Fig. S5), further confirming that the ionic currents measured in transformed vacuoles were mediated by *At*ALMT5 and *At*ALMT9. Since 1 mM $malate_{cyt}$ activates *At*ALMT9-mediated chloride currents (De Angeli *et al.*, 2013),

we tested whether it had the same effect on *At*ALMT5 (Fig. S4). We found that 1 mM malate$_{cyt}$ activated *At*ALMT5-mediated chloride currents inducing a 2.7 ± 0.8 time increase (Fig. S4). In the same conditions, *At*ALMT9 chloride currents were increased 4 ± 0.7 times (Fig. S4). Interestingly, we observed that, differently from *At*ALMT9, 1 mM fumarate$_{cyt}$ did not activate *At*ALMT5 chloride currents (Fig. S4).

The plant growth is not affected in *almt5* mutants

We selected two T-DNA knock-out lines, *almt5-1* and *almt5-2* (Figs 3a, S6a–c) in which the absence of the *At*ALMT5 mRNA expression was verified by reverse transcription quantitative polymerase chain reaction (Fig. S6d). In parallel, we generated the following complemented transgenic lines *almt5-1/gALMT5* and *almt5-1/gALMT5-GFP* (Figs 1c, S3, S6b,c). The expression of *AtALMT5* in *almt5-1/gALMT5* lines was confirmed by reverse transcription polymerase chain reaction (Fig. S6b,d) while in *almt5-1/gALMT5-GFP* by microscopy (Figs 1d, S3). Plants were grown under 8-h light regime for 40 d, and no development or growth defect was observed (Figs 3a, S7a). We quantified the rosette fresh weight (WT = 1.02 ± 0.22 g; *almt5-1* = 0.91 ± 0.20 g; *almt5-2* = 0.82 ± 0.24 g) and dry weight (WT = 0.15 ± 0.01 g; *almt5-1* = 0.07 ± 0.01 g; *almt5-2* = 0.06 ± 0.02 g), and no significant difference was found between WT and *almt5-1* or *almt5-2* (Figs 3b,c, S7b). To detect the effects on root growth, we grew WT, *almt5-1* and *almt5-2 in vitro* on agar plates, and we could not find any differences (Fig. S7c). These results were similar to previous reports made on knock-out lines for other vacuolar *At*ALMT channels where no growth defect was observed (Kovermann *et al.*, 2007; De Angeli *et al.*, 2013; Eisenach *et al.*, 2017; Ye *et al.*, 2021).

Mesophyll vacuoles from *almt5* mutants had reduced fumarate currents

We measured inward fumarate and malate currents in mesophyll vacuoles from *A. thaliana* WT, *almt5-1* and *almt5-2* plants. We performed patch-clamp experiments in the whole-vacuole configuration. We measured currents in vacuoles exposed to cytosolic side buffers containing either 100 mM malate$_{cyt}$ either 100 mM fumarate$_{cyt}$ (Fig. 4). In the presence of 100 mM malate$_{cyt}$ in WT, *almt5-1* and *almt5-2* vacuoles inward malate currents were not affected with a mean current density of −6 ± 4, −5 ± 2 and −6 ± 3 pA pF^{-1} at −127 mV, respectively (Fig. 4a). In the presence of 100 mM fumarate$_{cyt}$, WT vacuoles displayed inward rectifying currents with a mean current density of −28 ± 12 pA pF^{-1} at −127 mV (Fig. 4b). Like in *At*ALMT5 overexpressing vacuolar patches, Arabidopsis whole-vacuole fumarate inward currents did not present significant time-dependent components (Fig. 4b). In the presence of 100 mM fumarate$_{cyt}$, in *almt5-1* and *almt5-2* vacuoles, we measured inward currents densities of −10 ± 3 and −11 ± 3 pA pF^{-1} at −127 mV, respectively. This corresponds to a 64% and 61% reduction compared with WT vacuoles (Fig. 4b,d). Notably, the reduction in the inward fumarate currents occurs also at physiological membrane potentials (Fig. 4d). Therefore, mesophyll vacuoles from *almt5* mutants present a reduced capacity to mediate fumarate fluxes across the tonoplast, showing that *At*ALMT5 is involved in vacuolar fumarate transport.

*At*ALMT5 is not involved in the regulation of stomatal movements

Since *At*ALMT5 was expressed in guard cells (Figs 1a, S1l), such as *At*ALMT9 and *At*ALMT4 (De Angeli *et al.*, 2013; Eisenach *et al.*, 2017), we searched for a potential role of this ion channel in stomata regulation. We performed light-induced stomatal aperture experiment using leaf epidermis from WT, *almt5-1* and *almt5-2*. Isolated epidermis were incubated in a 30 mM KCl opening buffer at pH 5.7 and imaged before and after 3 h of light exposure (Fig. 5a). Stomatal apertures before (WT = 0.74 ± 0.10 µm; *almt5-1* = 0.69 ± 0.05 µm; *almt5-2* = 0.73 ± 0.09 µm) and after light exposure (WT = 1.47 ± 0.26 µm; *almt5-1* = 1.31 ± 0.22 µm; *almt5-2* = 1.35 ± 0.28 µm) were not significantly different between

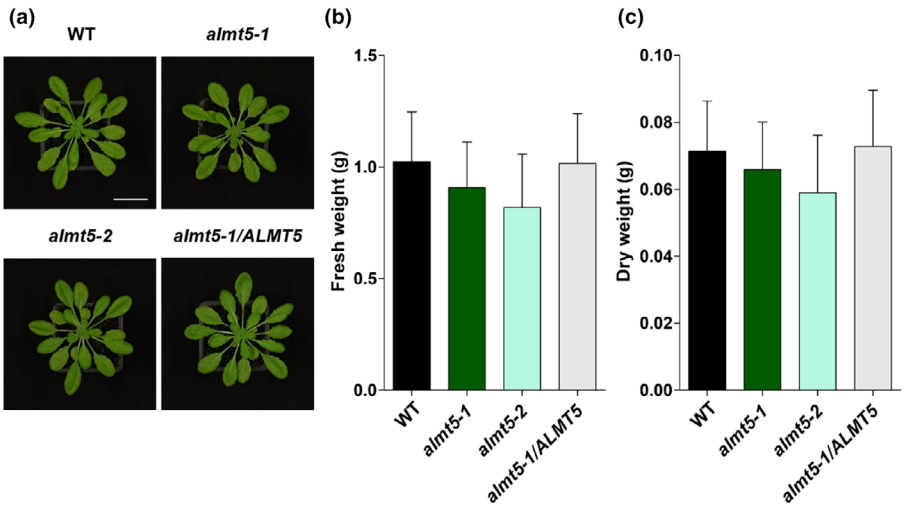

Fig. 3 Phenotypic analysis of *almt5-1* and *almt5-2* knock-out plants. (a) Wild-type (WT), *almt5-1*, *almt5-2* and *almt5-1/ALMT5 L5-3 Arabidopsis thaliana* 39-d-old plants grown in short days conditions (8-h light). Bar, 2 cm. (b) Rosette fresh weight of 40-d-old plants grown in the same conditions as in (a). Values are mean + SD, n = 10 for each genotype. (c) Rosette dry weight from (b). Values are mean + SD, n = 10 for each genotype. Statistical analysis: Mann–Whitney test, no significant differences between genotypes.

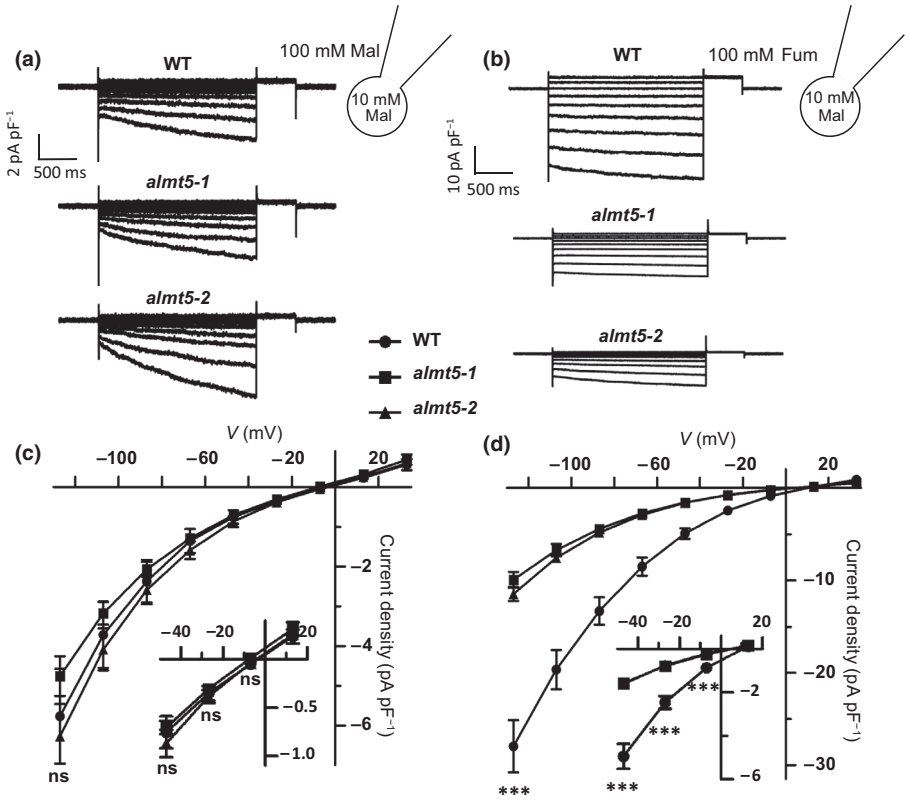

Fig. 4 *Arabidopsis thaliana* whole-vacuole patch-clamp analysis from wild-type (WT), *almt5-1* and *almt5-2* vacuoles. (a, b) Representative whole-vacuole currents from WT, *almt5-1* and *almt5-2* plants in cytosolic (cyt) malate$_{cyt}$ (a) and fumarate$_{cyt}$ (b) conditions. Starting from 0 mV, 2 s voltage steps from +33 mV until −127 mV in −20 mV decrements were applied, following each step a post-pulse at +33 mV for 500 ms was applied, holding potential was 0 mV. (c, d) *I/V* curves of the mean current densities in cytosolic malate (c; WT, closed circles, $n = 19$; *almt5-1*, closed squares, $n = 12$; *almt5-2*, closed triangle, $n = 13$) and fumarate conditions (d; WT, closed circles, $n = 12$; *almt5-1*, closed squares, $n = 11$; *almt5-2*, closed triangle, $n = 11$). Insets in (c, d) are magnifications of the *I/V* curves between +17 and −47 mV in presence of cytosolic malate or fumarate, respectively. Each data set is the mean ± SEM. Asterisks indicate statistically significant differences using the Mann–Whitney nonparametric test (***, $P < 0.001$).

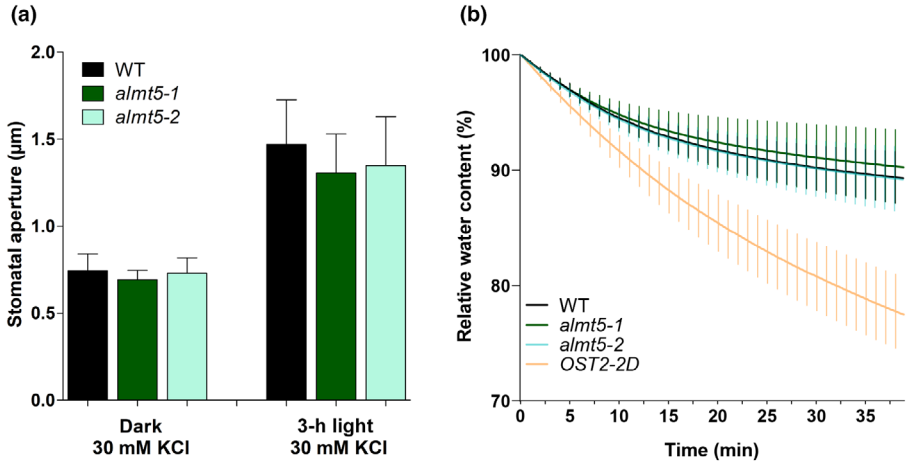

Fig. 5 Stomatal opening and closure is not modified in *almt5-1* and *almt5-2*. (a) Stomatal aperture measured in epidermal peels of *Arabidopsis thaliana* wild-type (WT) ($n = 15$ leaves from 15 plants), *almt5-1* ($n = 18$ leaves from 18 plants) and *almt5-2* ($n = 18$ leaves from 18 plants). Stomata were imaged in the dark and after 3 h of light exposure (240 µmol m^{-2} s^{-1}) in the presence of a 30 mM KCl buffer. Values are mean + SD. For each leaf, 40 stomata were analysed and used to calculate the mean leaf stomatal aperture. Statistical analysis with Mann–Whitney test shows no significant difference. (b) Relative water loss (FW − DW)/(FWi − DW) × 100 of Arabidopsis rosettes. After cutting the rosette, the fresh weight of WT ($n = 10$), *almt5-1* ($n = 10$), *almt5-2* ($n = 10$) and *OST2-2D* ($n = 7$) was measured for 40 min. Values are mean + SD. DW, dry weight; FW, fresh weight; FWi, initial fresh weight.

all genotypes. To test whether *At*ALMT5 was involved in stomatal closure, we conducted rosette dehydration experiments using WT, *almt5-1*, *almt5-2* and OST2-2D as positive control (Fig. 5b). The water loss measured in *almt5-1* and *almt5-2* was not significantly different from WT plants being 90.2 ± 3.3%, 89.1 ± 2.9% and 89.2 ± 2.3% after 40 min, respectively. The positive control OST2-2D mutants were strongly affected with a water loss of 77.1 ± 3.3% after 40 min (Fig. 5b). Therefore,

despite its expression in guard cells, under our experimental conditions, knocking-out *AtALMT5* did not affect stomatal aperture.

A modified C_4 organic acid balance in *almt5* mutants

In order to understand the function of *At*ALMT5, we investigated the content of the major inorganic (Cl^-, NO_3^-, PO_4^{3-}, SO_4^{2-}) and organic (malate, fumarate and citrate) anions in the leaves. Since malate and fumarate are accumulated during the day, we initially analysed their concentration in the middle of the photosynthetic period (i.e. 5-h illumination) when organic acids are already significantly accumulated in the leaves (Gibon *et al.*, 2009). We grew WT, *almt5-1*, *almt5-2*, *almt5/gALMT5* and *almt9-1* plants under short photoperiod (8-h light). We included *almt9-1* as a control since its organic anion levels does not differ from the WT (Baetz *et al.*, 2016). First, we found that the concentrations of NO_3^- (Fig. S8a), SO_4^{2-} (Fig. S8b) and Cl^- (Fig. S8c) were not significantly different in all the genotypes. Only, PO_4^{3-} was 15% higher in *almt9-1* plants (Fig. S8d).

Differently, we found significant differences in the organic acid contents. Indeed, we observed a 58% and 51% reduction of fumarate in *almt5-1* and *almt5-2* (7.0 ± 1.5 μmol g^{-1} FW and 8.0 ± 2.4 μmol g^{-1} FW, respectively) compared with WT (16.6 ± 4.9 μmol g^{-1} FW) (Fig. 6a). In parallel, in comparison with WT (11.4 ± 1.9 μmol g^{-1} FW), malate increased two times in *almt5-1* and *almt5-2* (*almt5-1* = 21.8 ± 3.2 μmol g^{-1} FW and *almt5-2* = 21.8 ± 5.4 μmol g^{-1} FW). The complemented plants *almt5-1/gALMT5* restored fumarate and malate to levels similar to the WT, confirming that the modification of C_4 acids content depends on *AtALMT5* (Fig. 6). Citrate contents, which is also stored in plant vacuoles, were similar in WT and *almt5* (WT = 16.7 ± 3.9, *almt5-1* = 17.3 ± 2.6 and *almt5-2* = 16.3 ± 4.2 μmol g^{-1} FW) (Fig. 6c). As previously reported, the *almt9-1* knock-out plants presented organic acids levels similar to the WT (Fig. 6; Baetz *et al.*, 2016). Interestingly, the sum of malate and fumarate contents in WT and *almt5* leaves was not significantly modified at the middle of the photoperiod (Fig. 6d). Consequently, also the C_4/citrate balance, which is highly regulated in plants (Lee *et al.*, 2021), was also not affected in *almt5-1* and *almt5-2*. Thus, the absence of *At*ALMT5 in the vacuolar membrane of mesophyll cells changed the balance between malate and fumarate stocks, two important carbon stores for Arabidopsis. The specific reduction in fumarate in *almt5* leaves strongly supports a role of *At*ALMT5 as an anion channel in transporting fumarate across the tonoplast of mesophyll cells. These findings in *almt5* were consistent with the patch-clamp results. Indeed, under physiological membrane potentials, fumarate currents directed to the vacuole were reduced in *almt5* mesophyll vacuoles (Fig. 4d *inset*).

Since malate and fumarate are stored along the all day period and degraded at night, we analysed the malate/fumarate balance at the end of day (ED) and at the end of the night (EN) (Table 1). In this experiment, we quantified other key carbon stores such as starch, glucose, fructose and sucrose (Table 2). As expected, malate and fumarate contents were higher in the leaves from ED than EN, consistent with previous reports (Gibon *et al.*, 2009). Similarly, to the data from plants collected at the middle of the photoperiod (Fig. 6), we found a modified malate and fumarate content in *almt5-1* (Table 1). At ED, fumarate was reduced by 66% while malate was increased by 32% compared with WT (Table 1). Similarly, at the EN, fumarate was 71% reduced and malate was 31% increased (Table 1). Interestingly, in this experiment, we found a reduction in the total C_4-organic acids content in *almt5-1* (ED-30% and EN-42%) compared with WT and *almt9-1* plants (Table 1). Notably, we did not find differences between the *almt5-1* and WT lines in starch, sucrose, fructose and glucose contents at ED or EN (Table 2).

In the cytosol of Arabidopsis mesophyll cells, malate is converted to fumarate by the FUM2 enzyme, which regulates the balance between these two C_4 acids (Pracharoenwattana *et al.*, 2010). The Arabidopsis knock-out mutants *fum2-1* and *fum2-2* display a dramatic reduction in the fumarate content (Pracharoenwattana *et al.*, 2010; Dyson *et al.*, 2016). We therefore compared fumarate contents between *almt5* and *fum2* mutants (Table S1). Interestingly, we found that in the *fum2-1* and *fum2-2*, fumarate was strongly reduced, while malate increased, confirming previously published data (Pracharoenwattana *et al.*, 2010; Dyson *et al.*, 2016). However, in *fum2-1* and *fum2-2*, the content of fumarate was 60% lower than in *almt5-1* or *almt5-2* (Table S1). Notably, in the *fum2* and *almt5* mutants, the malate content was increased compared with WT (Dyson *et al.*, 2016; Saunders *et al.*, 2022). This set of data shows that *almt5* mutants accumulate more fumarate than *fum2*. Moreover, the expression level of FUM2 is not modified in *almt5*, suggesting that FUM2 is active in *almt5* (Fig. S6). Thus, the fumarate reduction in *almt5* depends on a decreased fumarate transport across the tonoplast.

Discussion

The transport of organic acids such as malate, fumarate and citrate in the vacuole has been widely studied (Rentsch & Martinoia, 1991; Chia *et al.*, 2000; Hafke *et al.*, 2003; Hurth *et al.*, 2005). Indeed, these organic acids are accumulated into the vacuole of plant cells, where they serve as transient stores of carbon (Martinoia & Rentsch, 1994; Zell *et al.*, 2010; Saunders *et al.*, 2022). Malate, fumarate and citrate play key functions in plant metabolism, and they are stored in the vacuole to regulate their availability in metabolically active compartments. The first organic acid transport systems identified in the vacuole was *At*tDT, which works as a malate/citrate exchanger (Hurth *et al.*, 2005; Frei *et al.*, 2018). Later, a second group of membrane proteins, the *At*ALMTs, was identified (Sasaki *et al.*, 2004; Hoekenga *et al.*, 2006; Kovermann *et al.*, 2007). *At*ALMT4, *At*ALMT6 and *At*ALMT9 are able to mediate the transport of malate and fumarate, but not citrate, across the tonoplast (Meyer *et al.*, 2011; De Angeli *et al.*, 2013; Eisenach *et al.*, 2017). The vacuolar ALMTs mediate ionic currents through the vacuolar membrane resembling to the so-called 'malate currents', which were observed in other plant species (Pantoja & Smith, 2002;

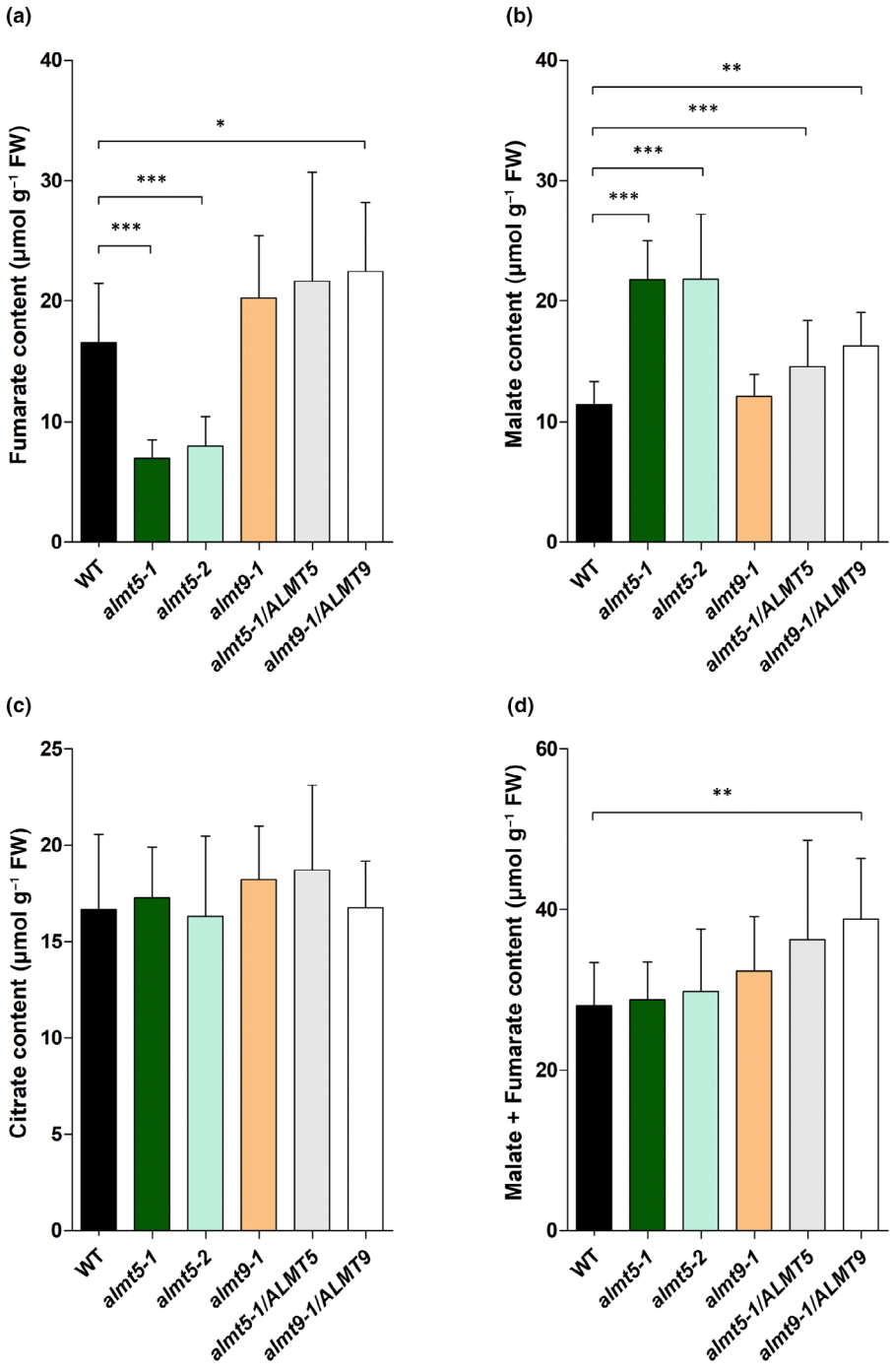

Fig. 6 Quantification of fumarate, malate and citrate in leaves. Organic anion contents measured by High Pressure Ion Chromatography (HPIC) in the leaves of *Arabidopsis thaliana* wild-type (WT), *almt5-1*, *almt5-2*, *almt9-1*, *almt5-1/gALMT5 L5-3* and *almt9-1/gALMT9 L4-3*. (a) fumarate, (b) malate, (c) citrate and (d) sum of malate + fumarate. Plants were 40-d-old grown in soil in short days conditions (8-h light), and leaves collected 5 h after the beginning of the light period. Values are mean + SD, $n = 12$ leaves from 12 plants of each genotype coming from two independent plant batches. Asterisks denote differences from the WT. Statistical analysis: Mann–Whitney test (*, $P < 0.05$; **, $P < 0.01$; ***, $P < 0.001$).

Hafke *et al.*, 2003). However, knocking out these vacuolar ALMTs in Arabidopsis has no impact on the accumulation of these organic acids (Baetz *et al.*, 2016) questioning their function *in vivo*. *At*ALMT5 is the only member of Clade II for which there is almost no information. In fact, apart from an early report suggesting an unclear localisation in the endomembranes (Kovermann *et al.*, 2007), no data are available on *At*ALMT5. The transient expression in tobacco of *AtALMT5-GFP cDNA* (Fig. S2b *bottom*) and the stable expression of *AtALMT5* genomic fragment fused to GFP in Arabidopsis (Figs 1b, S2c) demonstrated the localisation of *At*ALMT5 in the vacuolar membrane. At the plant level, *At*ALMT5 is expressed only in the shoots and, within the leaves, *At*ALMT5 is found in the guard cells, the mesophyll and epidermis (Figs 1a *middle*, S1i,j). Differently, *At*ALMT9 (Kovermann *et al.*, 2007) and *At*ALMT4 (Eisenach *et al.*, 2017) are expressed in the whole plant.

*At*ALMT5 presents specific ion transport properties

The comparative analysis of the ion currents mediated by *At*ALMT5 and *At*ALMT9 overexpressed in tobacco revealed that *At*ALMT5 is able to transport chloride, malate and fumarate like

Table 1 Malate, fumarate and citrate contents at the end of the dark and light periods.

	Malate		Fumarate		Malate + Fumarate		Citrate	
	EN	ED	EN	ED	EN	ED	EN	ED
WT	113.6 ± 17.5	158.3 ± 4.2	185.5 ± 33.6	288.8 ± 25.6	299.1 ± 49.0	447.0 ± 29.8	307.4 ± 36.4	236.9 ± 23.6
almt5-1	140.9 ± 9.3	235.0 ± 24.3**	56.9 ± 4.4**	96.6 ± 12.9**	197.8 ± 13.6**	331.7 ± 37.1**	305.3 ± 25.4	211.4 ± 17.6
almt9-1	99.6 ± 12.7	147.4 ± 9.0*	172.3 ± 21.7	278.6 ± 15.6	272.0 ± 34.1	426.0 ± 20.9	288.5 ± 21.9	212.0 ± 20.0
almt5-1/ALMT5	106.1 ± 19.3	159.3 ± 11.1	185.1 ± 48.2	238.2 ± 60.7	291.2 ± 64.9	397.5 ± 64.6	279.7 ± 43.1	236.2 ± 18.4
almt9-1/ALMT9	119.8 ± 12.8	170.5 ± 13.2	180.8 ± 27.3	235.8 ± 39.9	300.7 ± 38.3	406.3 ± 53.0	290.8 ± 30.4	207.2 ± 20.6

Organic acids contents in 40-d-old *Arabidopsis thaliana* rosette leaves of wild-type (WT), *almt5-1*, *almt9-1*, *almt5-1/ALMT5 L5-3* and *almt9-1/ALMT9 L4-3*. Data are from leaves collected at the end of day (ED) and end of night (EN). Each measurement corresponds to $n = 5$ replicates, each replicate correspond to a pool of three leaves from three plants. Data were obtained by HPIC. Data are mean ± SD. Statistical analysis: Mann–Whitney test (*, $P < 0.05$; **, $P < 0.01$). Asterisks represents a significant difference compared with the WT. Results are expressed in μmol g^{-1} DW.

Table 2 Soluble sugars and starch contents at the end of the dark and light periods.

	Glucose		Fructose		Sucrose		Starch	
	EN	ED	EN	ED	EN	ED	EN	ED
WT	24.3 ± 5.3	33.4 ± 3.8	14.5 ± 8.6	22.1 ± 3.7	15.2 ± 6.6	22.0 ± 8.6	107.4 ± 26.1	473.8 ± 76.8
almt5-1	31.0 ± 4.5	41.5 ± 8.2	17.0 ± 4.3	25.7 ± 8.9	9.0 ± 5.1	11.6 ± 6.1	129.2 ± 40.0	520.0 ± 95.6
almt9-1	27.8 ± 4.1	38.5 ± 6.1	12.4 ± 4.6	25.8 ± 4.7	7.6 ± 7.2	6.5 ± 4.5*	114.5 ± 32.7	526.5 ± 70.9
almt5-1/ALMT5	27.3 ± 1.7	35.6 ± 12.6	15.6 ± 3.9	28.1 ± 15.4	7.7 ± 3.4	22.7 ± 10.5	115.2 ± 29.3	481.4 ± 58.7
almt9-1/ALMT9	24.6 ± 6.7	35.3 ± 6.4	13.5 ± 6.9	24.0 ± 4.5	8.6 ± 5.2	10.1 ± 4.8*	102.4 ± 30.1	510.6 ± 56.6

Glucose, fructose, sucrose and starch contents in 40-d-old *Arabidopsis thaliana* rosette leaves of wild-type (WT), *almt5-1*, *almt9-1*, *almt5-1/ALMT5 L5-3* and *almt9-1/ALMT9 L4-3*. Data are from leaves collected at the end of day (ED) and end of night (EN). Each measurement corresponds to $n = 5$ replicates, each replicate correspond to a pool of three leaves from three plants. Data were obtained by the metaboHUB platform of Bordeaux. Data are mean ± SD. Statistical analysis: Mann–Whitney test (*, $P < 0.05$). Asterisks represents a significant difference compared with the WT. Results are expressed in μmol g^{-1} DW.

the other vacuolar ALMTs (De Angeli *et al.*, 2013; Eisenach *et al.*, 2017). Further, malate activates *At*ALMT5 chloride currents (Fig. S4), like for *At*ALMT4 and *At*ALMT9. However, cytosolic fumarate does not activate *At*ALMT5-GFP chloride currents (Fig. S4a,c).

The behaviour of *At*ALMT5 towards fumarate deviates from the other vacuolar *At*ALMTs (Fig. 2). In the presence of 100 mM cytosolic fumarate, differently from *At*ALMT9 and *At*ALMT6 (Meyer *et al.*, 2011), *At*ALMT5 does not present time-dependent kinetic (Fig. 2b). Indeed, *At*ALMT5 currents are immediately active right after the application of a voltage step (Fig. 2b; De Angeli *et al.*, 2013). The basis of the different functional properties of *At*ALMT5 and *At*ALMT9 is unknown, but they possibly rely on structural differences between the two proteins and future analysis might reveal the molecular basis. Notably, at physiological tonoplastic membrane potentials (i.e. 0 to −50 mV), *At*ALMT5 mediates only inward fumarate currents directed to the vacuolar lumen (Fig. 2c *inset*), while *At*ALMT9 transports both malate and fumarate (Fig. 2d *inset*). These data suggest that *At*ALMT5 mediates vacuolar fumarate loading. The analysis of malate and fumarate currents in Arabidopsis vacuoles confirmed a role of *At*ALMT5 transporting fumarate in the vacuolar lumen (Fig. 4). Indeed, vacuoles from WT and *almt5* presented typical inward malate currents (Hurth *et al.*, 2005; De Angeli *et al.*, 2013) with no differences between genotypes (Fig. 4a). However, in *almt5*, the vacuolar inward fumarate currents were lower than in WT at membrane potentials below 0 mV (Fig. 4b). Interestingly, like *At*ALMT5 currents in patches overexpressing *At*ALMT5, the fumarate currents measured in Arabidopsis WT vacuoles have no time-dependent component (Figs 2b, 4b). Thus, knocking out *AtALMT5* significantly reduced the capacity to mediate fumarate fluxes to the vacuolar lumen. Interestingly, the calculation of the divalent anion accumulation ratio between the vacuole and the cytosol that can be generated by an anion channel, like *At*ALMT5, shows a strong dependency on the membrane potential. With $pKa_1 = 3.03$ and $pKa_2 = 4.44$, fumarate is present as a divalent anion in both the cytosol (pH ≈ 7) and in the vacuole (pH ≈ 5.5–6) (Schnitzer *et al.*, 2011). Indeed, for divalent anion such as fumarate, the vacuole/cytosol accumulation ratio is five times at −20 mV and up 50 times at −50 mV. Thus, passive ion transport systems can mediate the vacuolar accumulation of divalent anions such as fumarate. Further, these data support the localisation of *At*ALMT5 in the tonoplast of Arabidopsis and show that it is specifically involved in the transport of fumarate in mesophyll cells.

*At*ALMT5 controls fumarate accumulation in the leaves

After the electrophysiological analysis, we quantified the anionic content of WT and *almt5* mutants in Arabidopsis leaves in the

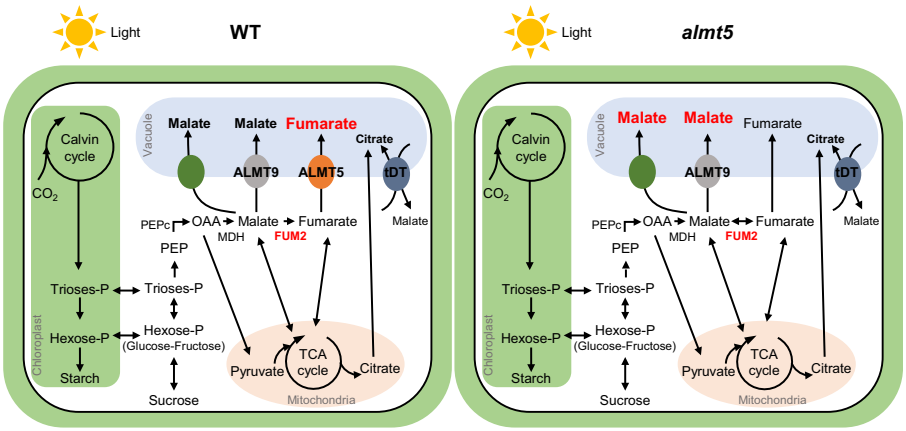

Fig. 7 Schematic of Aluminium-Activated Malate Transporter 5 (*At*ALMT5) function in malate and fumarate vacuolar loading. During daytime, malate and fumarate are produced and accumulated in the vacuole of *Arabidopsis thaliana*. In wild-type (WT; *left*), in the cytosol a part of the malate is converted into fumarate by FUM2. Malate and fumarate are transported from the cytosol to the vacuole by ion channels such as *At*ALMT9 and other transport systems such as *Att*DT. *At*ALMT5 specifically mediates fumarate accumulation in the vacuole. In *almt5* plants (*right*) where fumarate transport into the vacuole is reduced, the accumulation of this organic acid is reduced. The reduced capacity to transport fumarate in the vacuoles in *almt5* favours the accumulation of malate that is consequently increased. Therefore, *in almt5* plants, the malate/fumarate balance is modified. FUM2, FUMARASE2; MDH, malate dehydrogenase; OAA, oxaloacetate; PEP, phosphoenolpyruvate; PEPc, phosphoenolpyruvate carboxylase; TCA cycle, tricarboxylic acid cycle.

middle of photoperiod, at ED and at EN. We found that *almt5* plants accumulate less fumarate than WT plants (Fig. 6a; Table 1). Importantly, in *almt5* plants, concomitant with the fumarate decrease, malate increase (Tables 1, S1). The changes in the malate/fumarate balance do not result from an altered expression of other vacuolar malate transporters, such as *At*ALMT9 and *Att*DT (Fig. S6d,f). The reduction in fumarate is in line with patch-clamp data showing that *almt5* vacuoles have reduced fumarate transport capacity. Differently, *almt9-1* leaves present WT such as malate or fumarate levels like previously observed (Baetz *et al.*, 2016). Interestingly, citrate levels, which are tightly regulated (Lee *et al.*, 2021), remain stable in both *almt5* and *almt9-1* leaves, excluding a role of *At*ALMT5 and *At*ALMT9 in transporting citrate. The behaviour of *almt5* is reminiscent of the *fum2* plants lacking the cytosolic Fumarase2 (Table S1; Pracharoenwattana *et al.*, 2010), but in *almt5* plants, FUM2 expression level is similar to WT. Importantly, in *fum2* leaves, fumarate levels are three times lower than in *almt5*. This indicates that in *almt5* plants, FUM2 is active and that, despite the absence of *At*ALMT5, some fumarate is transported into the vacuole.

The residual accumulation of fumarate in *almt5* is likely mediated by other vacuolar *At*ALMTs or by *Att*DT (Fig. 7; Kovermann *et al.*, 2007; De Angeli *et al.*, 2013; Frei *et al.*, 2018). Interestingly, in *attdt*, knock-out malate and fumarate are reduced while citrate is increased (Medeiros *et al.*, 2017). Thus, *Att*DT leads to a nonspecific reduction of fumarate in the shoots. Differently, in *almt5* plants, we observed a specific reduction in fumarate (Fig. 6; Tables 1, S1). The total amount of dicarboxylic acids (i.e. malate + fumarate) in WT and *almt5* was similar in the middle of photoperiod (Fig. 6d; Table S1) but was reduced in *almt5* at ED and EN. Therefore, the absence of *At*ALMT5 reduces the fumarate transport capacity of the tonoplast, which significantly modifies the malate/fumarate balance and the total dicarboxylic acids levels at ED. However, like in *fum2* (Pracharoenwattana *et al.*, 2010; Dyson *et al.*, 2016), this reduction is not sufficient to impact on the biomass of *almt5*. Further, starch and soluble sugars contents were similar between the WT and *almt5* (Table 2), suggesting that the changed malate/fumarate balance in *almt5* does not modify the other carbon stocks (Fig. 7; Tcherkez *et al.*, 2012). These findings agree with the idea that fumarate accumulates in the vacuole as a fail-safe to keep malate homeostasis in the cytosol. In Arabidopsis, reducing the capacity to transport fumarate in the vacuole induces an unbalance of the malate/fumarate ratio in favour of malate.

Conclusion

In conclusion, we identified *At*ALMT5 as a malate and fumarate transport system, mediating the transport of fumarate into the vacuole of Arabidopsis mesophyll cells. Interestingly, this is the only example, among the vacuolar ALMTs, where knocking out the gene has a direct impact on the organic acid content of the leaves (Fig. 7; Baetz *et al.*, 2016; Eisenach *et al.*, 2017). This shows that *At*ALMT5 mediates fumarate transport in the tonoplast *in vivo*. Thus, the unique ion transport properties of *At*ALMT5 cannot be complemented by the other vacuolar *At*ALMTs present in *almt5*, opening the question of the effect of knocking out multiple vacuolar *At*ALMT. Finally, our results highlight the role of vacuolar ion transport systems in keeping cellular homeostasis. These data are a significant step forward to understand the homeostasis of organic acids in plant cells and open new perspectives on the regulation of the plant cell metabolism.

Acknowledgements

We thank Giles N. Johnson for kindly providing the *fum1-1* and *fum2-2* seeds. We thank Nathalie Leonhardt for providing us OST2-2D seeds. We thank S. Merlot for providing the pMOP

and pCOP vectors. We acknowledge the imaging facility MRI, member of the France – BioImaging national infrastructure supported by the French National Research Agency (ANR-10-INBS-04, «Investments for the future»), the Histocytology and Plant Cell Imaging platform (PHIV) and C. Alcon for assistance. We acknowledge the Plant Electrophysiology Platform (PEP) from the Institute for Plant Sciences of Montpellier (IPSiM) for technical support and assistance and C. Corratgé-Faille. We acknowledge the Isotope Quantification Platform (AQUI) and T. Perez assistance. This work was funded by CNRS grant (ATIP-Avenir) and the French National agency of Research (grant Netflux) to ADA. RD was funded by a PhD grant from University of Montpellier. PC-F was founded by a postdoctoral grant from Fundación Alfonso Martin Escudero and ANR Netflux. JJ was funded by CNRS.

Competing interests

None declared.

Author contributions

Imaging was performed RD, JJ and ADA. Ion, sugar and starch content was performed by RD with the assistance of PP, CC and PC-F. Molecular biology was performed by PC-F, JJ and ADA. Stomata aperture and dehydration experiments were done by RD with assistance from PC-F, data analysis by RD. Plant phenotyping and pictures were done by RD and PC-F. Patch-clamp experiments were done by JJ and EDC, and data analysis by JJ, ED-C and ADA. Selection of knock-out mutants and gene expression was done by PC-F. Selection of transgenic lines was done by KB, PC-F and JJ. ADA and RD wrote the manuscript with the contribution of PC-F. ADA conceived the research with the contribution of RD, PC-F. RD, JJ and PC-F contributed equally to this work.

ORCID

Cédric Cassan https://orcid.org/0000-0003-3022-4278
Paloma Cubero-Font https://orcid.org/0000-0002-0231-9811
Alexis De Angeli https://orcid.org/0000-0003-3072-7932
Elsa Demes-Causse https://orcid.org/0000-0002-8386-7763
Roxane Doireau https://orcid.org/0009-0005-8993-8998
Justyna Jaślan https://orcid.org/0000-0002-1620-912X
Pierre Pétriacq https://orcid.org/0000-0001-8151-7420

Data availability

All relevant data supporting the findings of this study are available in this article and in the Supporting Information (Figs S1–S8; Methods S1; Tables S1, S2).

References

Araújo WL, Nunes-Nesi A, Fernie AR. 2011. Fumarate: multiple functions of a simple metabolite. *Phytochemistry* **72**: 838–843.

Baetz U, Eisenach C, Tohge T, Martinoia E, De Angeli A. 2016. Vacuolar chloride fluxes impact ion content and distribution during early salinity stress. *Plant Physiology* **172**: 1167–1181.

Bertl A, Blumwald E, Coronado R, Eisenberg R, Findlay G, Gradmann D, Hille B, Köhler K, Kolb HA, MacRobbie E *et al.* 1992. Electrical measurements on endomembranes. *Science* **258**: 873–874.

Biais B, Bénard C, Beauvoit B, Colombié S, Prodhomme D, Ménard G, Bernillon S, Gehl B, Gautier H, Ballias P *et al.* 2014. Remarkable reproducibility of enzyme activity profiles in tomato fruits grown under contrasting environments provides a roadmap for studies of fruitmetabolism. *Plant Physiology* **164**: 1204–1221.

Carpaneto A, Boccaccio A, Lagostena L, Di Zanni E, Scholz-Starke J. 2017. The signaling lipid phosphatidylinositol-3,5-bisphosphate targets plant CLC-a anion/H^+ exchange activity. *EMBO Reports* **18**: 1100–1107.

Cheung CYM, Poolman MG, Fell DA, George Ratcliffe R, Sweetlove LJ. 2014. A diel flux balance model captures interactions between light and dark metabolism during day-night cycles in C_3 and crassulacean acid metabolism leaves. *Plant Physiology* **165**: 917–929.

Chia DW, Yoder TJ, Reiter WD, Gibson SI. 2000. Fumaric acid: an overlooked form of fixed carbon in Arabidopsis and other plant species. *Planta* **211**: 743–751.

Clough SJ, Bent AF. 1998. Floral dip: a simplified method for *Agrobacterium*-mediated transformation of *Arabidopsis thaliana*. *The Plant Journal* **16**: 735–743.

Curtis MD, Grossniklaus U. 2003. A gateway cloning vector set for high-throughput functional analysis of genes *in planta*. *Plant Physiology* **133**: 462–469.

De Angeli A, Zhang J, Meyer S, Martinoia E. 2013. AtALMT9 is a malate-activated vacuolar chloride channel required for stomatal opening in Arabidopsis. *Nature Communications* **4**: 1–10.

Dyson BC, Miller MAE, Feil R, Rattray N, Bowsher CG, Goodacre R, Lunn JE, Johnson GN. 2016. FUM2, a cytosolic fumarase, is essential for acclimation to low temperature in *Arabidopsis thaliana*. *Plant Physiology* **172**: 118–127.

Eisenach C, Baetz U, Huck NV, Zhang J, De Angeli A, Beckers GJM, Martinoia E. 2017. ABA-induced stomatal closure involves ALMT4, a phosphorylation-dependent vacuolar anion channel of Arabidopsis. *Plant Cell* **29**: 2552–2569.

Fernie AR, Martinoia E. 2009. Malate. Jack of all trades or master of a few? *Phytochemistry* **70**: 828–832.

Frei B, Eisenach C, Martinoia E, Hussein S, Chen XZ, Arrivault S, Neuhaus HE. 2018. Purification and functional characterization of the vacuolar malate transporter tDT from Arabidopsis. *Journal of Biological Chemistry* **293**: 4180–4190.

Gibon Y, Pyl ET, Sulpice R, Lunn JE, Höhne M, Günther M, Stitt M. 2009. Adjustment of growth, starch turnover, protein content and central metabolism to a decrease of the carbon supply when Arabidopsis is grown in very short photoperiods. *Plant, Cell & Environment* **32**: 859–874.

Gibon Y, Vigeolas H, Tiessen A, Geigenberger P, Stitt M. 2002. Sensitive and high throughput metabolite assays for inorganic pyrophosphate, ADPGIc, nucleotide phosphates, and glycolytic intermediates based on a novel enzymic cycling system. *The Plant Journal* **30**: 221–235.

Hafke JB, Hafke Y, Smith JAC, Lüttge U, Thiel G. 2003. Vacuolar malate uptake is mediated by an anion-selective inward rectifier. *The Plant Journal* **35**: 116–128.

Heazlewood JL, Millar AH. 2005. AMPDB: the Arabidopsis mitochondrial protein database. *Nucleic Acids Research* **33**: 605–610.

Hoekenga OA, Maron LG, Piñeros MA, Cançado GMA, Shaff J, Kobayashi Y, Ryan PR, Dong B, Delhaize E, Sasaki T *et al.* 2006. AtALMT1, which encodes a malate transporter, is identified as one of several genes critical for aluminum tolerance in Arabidopsis. *Proceedings of the National Academy of Sciences, USA* **103**: 9738–9743.

Hurth MA, Su JS, Kretzschmar T, Geis T, Bregante M, Gambale F, Martinoia E, Neuhaus HE. 2005. Impaired pH homeostasis in Arabidopsis lacking the vacuolar dicarboxylate transporter and analysis of carboxylic acid transport across the tonoplast. *Plant Physiology* **137**: 901–910.

Jefferson RA. 1987. Assaying chimeric genes in plants: the GUS gene fusion system. *Plant Molecular Biology Reporter* **5**: 387–405.

Kaufmann K, Pajoro A, Angenent GC. 2010. Regulation of transcription in plants: mechanisms controlling developmental switches. *Nature Reviews Genetics* **11**: 830–842.

Konrad KR, Hedrich R. 2008. The use of voltage-sensitive dyes to monitor signal-induced changes in membrane potential-ABA triggered membrane depolarization in guard cells. *The Plant Journal* **55**: 161–173.

Kovermann P, Meyer S, Hörtensteiner S, Picco C, Scholz-Starke J, Ravera S, Lee Y, Martinoia E. 2007. The Arabidopsis vacuolar malate channel is a member of the ALMT family. *The Plant Journal* **52**: 1169–1180.

Lee CP, Elsässer M, Fuchs P, Fenske R, Schwarzländer M, Millar AH. 2021. The versatility of plant organic acid metabolism in leaves is underpinned by mitochondrial malate-citrate exchange. *Plant Cell* **33**: 3700–3720.

Li C, Dougherty L, Coluccio AE, Meng D, El-Sharkawy I, Borejsza-Wysocka E, Liang D, Piñeros MA, Xu K, Cheng L. 2020. Apple ALMT9 requires a conserved C-terminal domain for malate transport underlying fruit acidity. *Plant Physiology* **182**: 992–1006.

Luna E, Flandin A, Cassan C, Prigent S, Chevanne C, Kadiri CF, Gibon Y, Pétriacq P. 2020. Metabolomics to exploit the primed immune system of tomato fruit. *Metabolites* **10**: 96.

Martinoia E, Maeshima M, Neuhaus HE. 2007. Vacuolar transporters and their essential role in plant metabolism. *Journal of Experimental Botany* **58**: 83–102.

Martinoia E, Rentsch D. 1994. Compartmentation-responses to a complex metabolism. *Plant Physiology* **45**: 447–467.

Maruyama H, Sasaki T, Yamamoto Y, Wasaki J. 2019. AtALMT3 is involved in malate efflux induced by phosphorus deficiency in *Arabidopsis thaliana* root hairs. *Plant and Cell Physiology* **60**: 107–115.

Medeiros DB, Barros KA, Barros JAS, Omena-Garcia RP, Arrivault S, Sanglard LMVP, Detmann KC, Silva WB, Daloso DM, Damatt FM *et al.* 2017. Impaired malate and fumarate accumulation due to the mutation of the tonoplast dicarboxylate transporter has little effects on stomatal behavior. *Plant Physiology* **175**: 1068–1081.

Merlot S, Leonhardt N, Fenzi F, Valon C, Costa M, Piette L, Vavasseur A, Genty B, Boivin K, Müller A *et al.* 2007. Constitutive activation of a plasma membrane H^+-ATPase prevents abscisic acid-mediated stomatal closure. *EMBO Journal* **26**: 3216–3226.

Meyer S, Mumm P, Imes D, Endler A, Weder B, Al-Rasheid KAS, Geiger D, Marten I, Martinoia E, Hedrich R. 2010. AtALMT12 represents an R-type anion channel required for stomatal movement in Arabidopsis guard cells. *The Plant Journal* **63**: 1054–1062.

Meyer S, Scholz-Starke J, De Angeli A, Kovermann P, Burla B, Gambale F, Martinoia E. 2011. Malate transport by the vacuolar AtALMT6 channel in guard cells is subject to multiple regulation. *The Plant Journal* **67**: 247–257.

Muller B, Pantin F, Génard M, Turc O, Freixes S, Piques M, Gibon Y. 2011. Water deficits uncouple growth from photosynthesis, increase C content, and modify the relationships between C and growth in sink organs. *Journal of Experimental Botany* **62**: 1715–1729.

Pantoja O, Smith JAC. 2002. Sensitivity of the plant vacuolar malate channel to pH, Ca^{2+} and anion-channel blockers. *Journal of Membrane Biology* **186**: 31–42.

Pracharoenwattana I, Zhou W, Keech O, Francisco PB, Udomchalothorn T, Tschoep H, Stitt M, Gibon Y, Smith SM. 2010. Arabidopsis has a cytosolic fumarase required for the massive allocation of photosynthate into fumaric acid and for rapid plant growth on high nitrogen. *The Plant Journal* **62**: 785–795.

Rentsch D, Martinoia E. 1991. Citrate transport into barley mesophyll vacuoles – comparison with malate-uptake activity. *Planta* **184**: 532–537.

Roelfsema MRG, Hedrich R. 2005. In the light of stomatal opening: new insights into 'the Watergate'. *New Phytologist* **167**: 665–691.

Sasaki T, Ariyoshi M, Yamamoto Y, Mori IC. 2022. Functional roles of ALMT-type anion channels in malate-induced stomatal closure in tomato and Arabidopsis. *Plant, Cell & Environment* **45**: 2337–2350.

Sasaki T, Yamamoto Y, Ezaki B, Katsuhara M, Ahn SJ, Ryan PR, Delhaize E, Matsumoto H. 2004. A wheat gene encoding an aluminum-activated malate transporter. *The Plant Journal* **37**: 645–653.

Saunders HA, Calzadilla PI, Schwartz JM, Johnson GN. 2022. Cytosolic fumarase acts as a metabolic fail-safe for both high and low temperature acclimation of *Arabidopsis thaliana*. *Journal of Experimental Botany* **73**: 2112–2124.

Schnitzer D, Seidel T, Sander T, Golldack D, Dietz KJ. 2011. The cellular energization state affects peripheral stalk stability of plant vacuolar H^+-ATPase and impairs vacuolar acidification. *Plant and Cell Physiology* **52**: 946–956.

Sharma T, Dreyer I, Kochian L, Piñeros MA. 2016. The ALMT family of organic acid transporters in plants and their involvement in detoxification and nutrient security. *Frontiers in Plant Science* **7**: 1–12.

Tcherkez G, Boex-Fontvieille E, Mahé A, Hodges M. 2012. Respiratory carbon fluxes in leaves. *Current Opinion in Plant Biology* **15**: 308–314.

Winter K, Smith JAC. 2022. CAM photosynthesis: the acid test. *New Phytologist* **233**: 599–609.

Ye W, Koya S, Hayashi Y, Jiang H, Oishi T, Kato K, Fukatsu K, Kinoshita T. 2021. Identification of genes preferentially expressed in stomatal guard cells of *Arabidopsis thaliana* and involvement of the aluminum-activated malate transporter 6 vacuolar malate channel in stomatal opening. *Frontiers in Plant Science* **12**: 1–8.

Zell MB, Fahnenstich H, Maier A, Saigo M, Voznesenskaya EV, Edwards GE, Andreo C, Schleifenbaum F, Zell C, Drincovich MF *et al.* 2010. Analysis of Arabidopsis with highly reduced levels of malate and fumarate sheds light on the role of these organic acids as storage carbon molecules. *Plant Physiology* **152**: 1251–1262.

Zhang J, Baetz U, Krügel U, Martinoia E, De Angeli A. 2013. Identification of a probable pore-forming domain in the multimeric vacuolar anion channel AtALMT9. *Plant Physiology* **163**: 830–843.

Supporting Information

Additional Supporting Information may be found online in the Supporting Information section at the end of the article.

Fig. S1 Aluminium-Activated Malate Transporter 5 promoter activity reported by β-glucuronidase staining.

Fig. S2 Subcellular localisation of Aluminium-Activated Malate Transporter 5.

Fig. S3 Expression pattern of Aluminium-Activated Malate Transporter 5.

Fig. S4 Activation of Aluminium-Activated Malate Transporter 5 (*At*ALMT5) and *At*ALMT9 chloride currents by organic acids.

Fig. S5 Vacuolar ionic currents from *Nicotiana benthamiana* transformed with empty vectors.

Fig. S6 Aluminium-Activated Malate Transporter 5 gene structure and mRNA expression of *ALMT5*, *ALMT9*, *tDT* and *FUM2* in *Arabidopsis thaliana* leaves.

Fig. S7 *almt5* biomass and root growth phenotype.

Fig. S8 Inorganic contents in *Arabidopsis thaliana* wild-type, *almt5-1*, *almt5-2*, *almt9-1* and complemented lines.

Methods S1 Supporting methods.

Table S1 Organic and inorganic anions contents.

Table S2 List of primers.

Please note: Wiley is not responsible for the content or functionality of any Supporting Information supplied by the authors. Any queries (other than missing material) should be directed to the *New Phytologist* Central Office.